ELSEVIER

Contents lists available at ScienceDirect

# Acta Biomaterialia

journal homepage: www.elsevier.com/locate/actbio



# Full length article

# Molecular and skeletal fingerprints of scleractinian coral biomineralization: From the sea surface to mesophotic depths<sup>★</sup>



Assaf Malik<sup>a,b</sup>, Shai Einbinder<sup>c</sup>, Stephane Martinez<sup>b,c</sup>, Dan Tchernov<sup>b,c</sup>, Sivan Haviv<sup>b,d</sup>, Ricardo Almuly<sup>b</sup>, Paul Zaslansky<sup>e</sup>, Iryna Polishchuk<sup>f</sup>, Boaz Pokroy<sup>f</sup>, Jarosław Stolarski<sup>g</sup>, Tali Mass<sup>b,\*</sup>

- <sup>a</sup> Bioinformatics Core Unit, University of Haifa, Haifa, Israel
- <sup>b</sup> Department of Marine Biology, The Leon H. Charney School of Marine Sciences, University of Haifa, Mt. Carmel, Haifa 3498838, Israel
- <sup>c</sup> Morris Kahn Marine Research Station, University of Haifa, Shdot Yam, Israel
- <sup>d</sup> The Interuniversity Institute of Marine Sciences, Eilat 88103, Israel
- <sup>e</sup> Center for Dental and Craniofacial Sciences, Charite University Hospital, Berlin, Germany
- <sup>f</sup> Department of Materials Science and Engineering and the Russel Berrie Nanotechnology Institute, Technion-Israel Institute of Technology, 32000 Haifa,
- g Institute of Paleobiology, Polish Academy of Sciences, Twarda 51/55, 00-818, Warsaw, Poland

#### ARTICLE INFO

Article history:
Received 26 September 2019
Revised 16 December 2019
Accepted 9 January 2020
Available online 16 January 2020

Keywords:
Bioinfomatics/phyloinfomatics
Cnidarians
Mesophotic reef
Biomineralization
Morphology plasticity
Electron microscopy
Micro ct
High-resolution synchrotron x-ray powder
diffraction

#### ABSTRACT

Reef-building corals, the major producers of biogenic calcium carbonate, form skeletons in a plethora of morphological forms. Here we studied skeletal modifications of Stylophora pistillata (clade 4) colonies that adapt to increasing depths with decreasing ambient light. The coral show characteristic transitions from spherical morphologies (shallow depths, 5 m deep) to flat and branching geometries (mesophotic depths, 60 m deep). Such changes are typically ascribed to the algal photosymbiont physiological feedback with the coral that host them. We find specific fine-scale skeletal variability in accretion of structure at shallow- and mesophotic depth morphotypes that suggest underlying genomic regulation of biomineralization pathways of the coral host. To explain this, we conducted comparative morphology-based analyses, including optical and electron microscopy, tomography and X-ray diffraction analysis coupled with a comprehensive transcriptomic analysis of S. pistillata. The samples originated from Gulf of Eilat in the Red Sea collected along a depth gradient from shallow to mesophotic depths (5 to 60 m). Additional samples were experimentally transplanted from 5 m to 60 m and from 60 m to 5 m. Interestingly, both morphologically and functionally, transplanted corals partly adapt by exhibiting typical depth-specific properties. In mesophotic depths, we find that the organic matrix fraction is enriched in the coralla, well matching the overrepresentation of transcripts encoding biomineralization "tool-kit" structural extracellularproteins that was observed. These results provide insights into the molecular mechanisms of calcification and skeletal adaptation that repeatedly allowed this coral group to adapt to a range of environments presumably with a rich geological past.

### Statement of Significance

Understanding the reef coral physiological plasticity under a rapidly changing climate is of crucial importance for the protection of coral reef ecosystems. Most of the reef corals operate near their upper limit of heat tolerance. A possible rescue for some coral species is migration to deeper, cooler mesophotic depths. However, gradually changing environmental parameters (especially light) along the depth gradient pose new adaptative stress on corals with largely unknown influences on the various biological molecular pathways. This work provides a first comprehensive analysis of changes in gene expression, including biomineralization "tool kit" genes, and reports the fine-scale microstructural and crystallographic skeletal details in *S. pistillata* collected in the Red Sea along a depth gradient spannign 5 to 60 m.

© 2020 Acta Materialia Inc. Published by Elsevier Ltd. All rights reserved.

E-mail address: tmass@univ.haifa.ac.il (T. Mass).

<sup>\*</sup> Part of the Special Issue on Biomineralization: From Cells to Biomaterials, associated with the BIOMIN XV: 15th International Symposium on Biomineralization, held at the Ludwig Maximilian University, Sept 9-13, 2019, organized by Wolfgang Schmahl and Erika Griesshaber.

<sup>\*</sup> Corresponding author.

#### 1. Introduction

Many organisms across the tree of life are capable of forming mineral deposits that play important structural roles [1]. In most cases, biomineralization is a biologically controlled process of mineral formation and the resulting biogenic minerals (or biominerals) are used in a variety of functions, ranging from magnetic compasses used for navigation to skeletons providing mechanical support and protection [2]. The morphology, mineralogy and chemistry of biologically formed minerals depend on both the organism and the environmental surroundings. Genetically controlled structural proteins and enzymes act as key contributors to control the internal, physiological conditions, responding to external environmental parameters [3]. This holds also for calcium carbonate (CaCO<sub>3</sub>), one of the most abundant minerals found in nature. Indeed the reef-building scleractinian corals belong to the most extensive producers of the biogenic form of this mineral. The scleractinian coral skeleton which is used as a structural and/or protective material [4], consists of mainly inorganic CaCO<sub>3</sub> in the form of aragonite, and a minor organic phase. This organic phase (or skeletal organic matrix, SOM) consist of various macromolecules such as polysaccharides, lipids, and proteins [5] that are used by the coral to modulate biomineralization and become entrapped in the skeleton [6].

To deepen knowledge about coral biomineralization it is important to understand the interplay between biological and environmental factors that influence the skeletal form and structure at different length-scales (from macromorphology to fine-scale structures). Although coral skeletons have a characteristic architecture, each species has macromorphological distinct characteristics, and coral morphologies may also significantly vary along environmental gradients [7]. This represents an adaptive capacity referred as phenotypic plasticity, allowing the coral organism to produce a range of relatively fit phenotypes by altering morphology, state, movement, life history or behavior in relation to variations in biotic and abiotic environmental parameters [8-10]. It is impressive that related taxa of sessile coral are capable of inhabiting a wide range of environments due to phenotypic plasticity. Consequently, individual colonies representing the same genetic population can significantly vary in morphology, physiology, and biomineralization behavior that are affected by environmental conditions. Previous studies demonstrated for example that morphological plasticity of scleractinian corals may be induced by differences in water flow [11-13], depth [14,15], or other environmental (e.g. light, temperature) parameters [16]. It was also shown that different species may develop morphologies that are similar to other species when transplanted to the common environment: e.g., Pocillopora meandrina can develop morphological features typical to Pocillopora damicornis when examined several months after reciprocal transplantation to the same locality [17].

One example of scleractinian coral phenotypic plasticity is Stylophora pistillata, a common widely-distributed and extensivelystudied species of branching coral, with a wide bathymetric distribution. S. pistillata typically dwell in the shallowest reefs (sea surface) but have been found in the mesophotic zone (up to 70 m) which is at the lower limit of light penetration in sea water (in the Red Sea the mesophotic zone extends between 40 and 150 m). The mesophotic environment exposes its inhabitants to physical conditions that are different from those in shallower reefs and the physical conditions change in several ways. These include reduced light intensity levels [18], a narrower optical spectrum [19], cooler temperatures, absence of coastal wave effect, different nutrient concentration and higher hydrostatic pressures [20]. These changes create a different environment for corals to grow in, increasing the need for adaptation e.g., to optimize potential light harvesting and food capturing [14]. Einbinder et al. [14] reported that S. pistillata changes from a hemispherical shape with thick branches (shallow-water) to planar colonies with thinner branches (deeperwater). In addition, the corallite, i.e., the skeletal "cup" in which the coral polyp resides, exhibits a decrease in diameter, while the spacing between polyps increases with depth. Moreover, both photosynthesis of the symbiotic algae (zooxanthellae) and calcification rates decrease with depth [18] and the coral diet changes towards a more heterotrophic form of nutrition [14]. Some aspects of the influence of zooxanthellae activity on coral biomineralization can be associated with a phenomenon known as light-enhanced calcification [21] which may explain the lower calcification rates in mesophotic corals [20]. However, recent progress in understanding the genomic regulation of the biomineralization process calls for a much more comprehensive explanation of changes in coral biomineralization observed along a depth gradient.

The purpose of this study is to track changes in gene expression, including biomineralization "tool kit" genes, and to map finescale microstructural and crystallographic skeletal details in the Red Sea S. pistillata found between 5 and 60 m below sea level. In addition to systematic observations of corals derived from different depths, a long-term reciprocal transplantation experiment was performed, exchanging shallow-water corals (5 m) with corals from mesophotic depths (60 m) for 3 or 15 months. The aim of this experiment was to assess if the development of fine-scale morphological features typical to shallow or mesophotic morphotypes is genomically regulated as a response to environmental changes, and by which biomineralization and developmental genes. The study provides a unique opportunity to understand relationships between biomineralization "tool kit" gene expression and fine-scale structural features of the skeleton in one coral species. As such, our approach may even pave the way for new interpretations of fossil coral micromorphology (including fossil Stylophora species).

### 2. Results

Visual inspection while diving in the Gulf of Eilat/Aqaba reveals that with increasing depth, colonies of Stylophora pistillata change the shape from being spherical thick branched in shallow-waters to exhibiting table like thin branched morphotypes in mesophotic depths [14] (Fig 1A-G). The newly grown area (labeled with alizarin red) of S. pistillata transplanted from 60 m to 5 m or from 5 m to 60 m did not show a significant change in colony morphology after 3 months (Fig. 1I, left photo, Fig. S1). However, the colonies transplanted form 60 m to 5 m started to develop spherical shapes similar to the morphotype of shallow depth colonies after a year (Fig. 1I, right photo, Fig. S1). The colonies transplanted from 5 m to 60 m (Fig. 1]) became completely overgrown by tunicates and died before we could compare their morphology after one year. Differences in morphology are often considered to be indicative of separate morphospecies existing along this depth gradient. Therefore, to exclude the possibility that the differences observed along the depth gradient are due to a sampling of different molecular clades we performed phylogenetic analyses using mitochondrial Cytochrome Oxidase I (COI) DNA barcoding primers [22]. This analysis revealed that all studied colonies belong to Red Sea clade 4. This clade is found throughout the northwest Indian Ocean including the Red Sea, the Persian/Arabian Gulf and Kenya [22] (Fig. 1H).

# 2.1. Skeleton characteristics of Stylophora pistillata along the depth gradient

The corallite morphology of the colonies collected from the different depths is fully comparable with the morphology of corallites of *S. pistillata* clade 4 described by Keshavmurthy et al. [22]. The corallites exhibit six poorly-developed septa not fused with columella and that are continuous with the hoods in the coenosteum

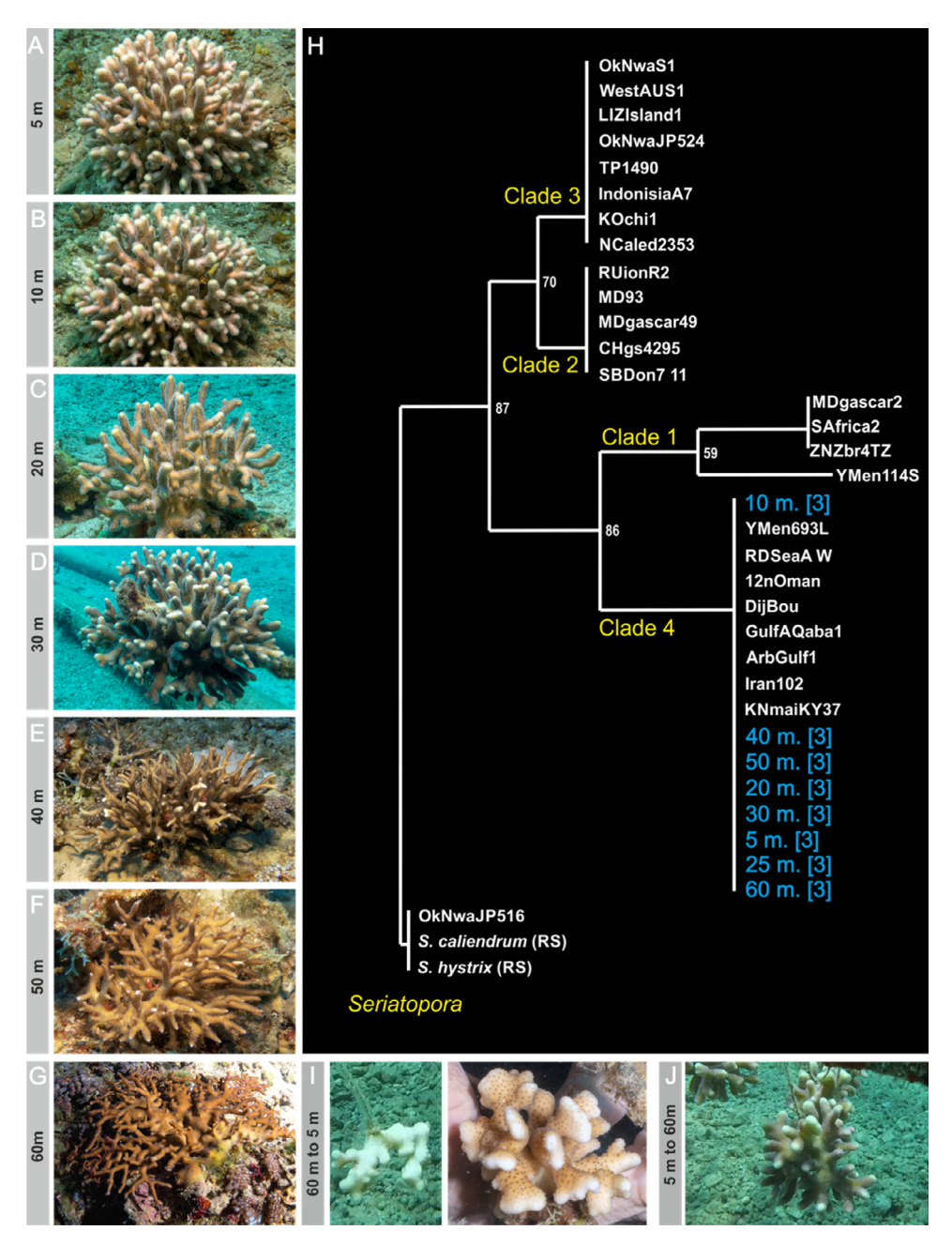


**Fig. 1.** Macromorphological and molecular characteristics of shallow to deep-water and transplanted morphotypes of *S. pistillata* scleractinian coral. (A–G, I–J) Overall colony shapes: shallow-water morphotypes form spherical colonies whereas deeper-water ones are flatter. The 5 to 60 m transplanted colonies were imaged 3 months after reciprocal transplantation, while the 60 to 5 m colonies were imaged 3 and 15 months after reciprocal transplantation (I, left and right respectively). (H) The phylogenetic tree of *S. pistallata* based on COI gene sequences. All specimens of *S. pistallata* collected along the depth gradient (highlighted text) and used in this study are the members of clade 4; COI sequences of other *Stylophora* clades are given after [16]. Bootstrap values are shown at tree nodes. (For interpretation of the references to color in this figure legend, the reader is referred to the web version of this article.)

(Fig. 2A). However, similar to the observation of Einbinder et al. [14] we found that the spatial relationship between corallites and coenosteum is clearly different in colonies collected from different depths (Fig. 3, Fig. 4A Movies S1-S4). The diameters of the corallites significantly decrease from 0.93  $\pm$  0.08 to 0.53  $\pm$  0.05 mm at 5 vs. 60 m respectively, while the distances between calices, or coenosteal areas increase from 0.51  $\pm$  0.13 to 1.38  $\pm$  0.44 mm at 5 vs. 60 m respectively (Fig. 4A, Table S1). Nonetheless, this trait did not change significantly after translocating the colonies from 5 m to 60 m or from 60 m to 5 m after 3 months (Fig. 3H, I, Fig. 4A, Table S1). Within one year after transplantation, the morphology of the colonies moved form 60 m to 5 m become significantly more similar to the shallow depth colonies (Fig. 3J, Fig. 4A,

Table S1). Moreover, the coenosteal spines in shallow-water forms are significantly longer (sections in Fig. 2C, yellow arrows) and have a larger area with granular texture (Fig. 2B, red-transparent) as compared with the mesophotic depths ones. The ratio between the granular (Fig. 2B, red-transparent) and the smoother (Fig. 2B, blue-transparent) zones of the spine significantly decreases from  $1.4 \pm 0.33$  to  $0.7 \pm 0.18$  at 5 and 60 m respectively (Fig. 2B, Fig. 4A, Table S1). Moreover, the spine structure of the colonies transplanted from 60 m to 5 m (60  $\rightarrow$  5 m) is similar to those grown at 60 m depths, whereas the spines of the colonies that were transplanted from 5 m to 60 m (5  $\rightarrow$  60)resemble those of 60 m morphotypes (Fig. 4A). The fine-scale granulae on coeanosteal spines correspond to Rapid Accretion Deposits (RAD) or Center of

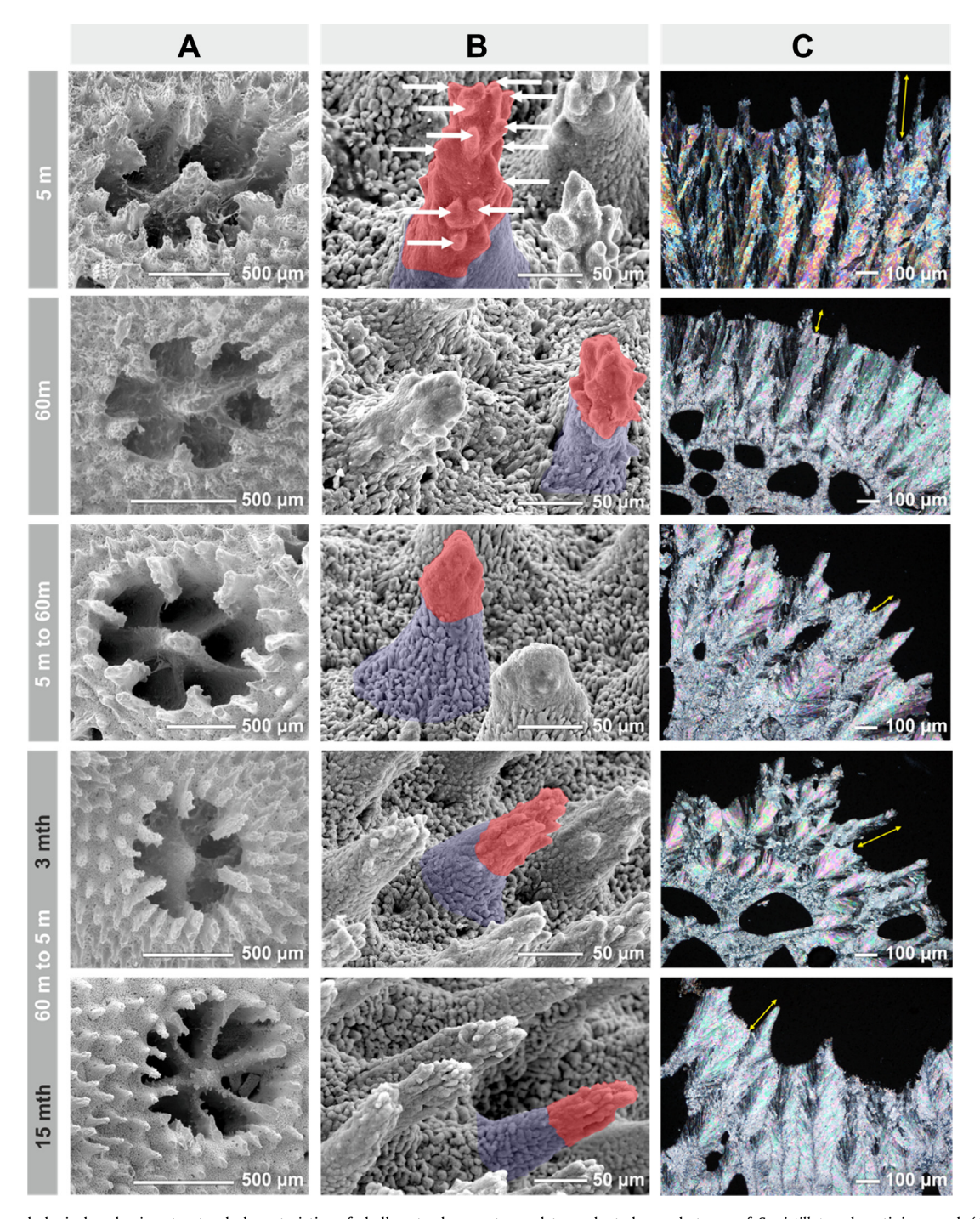


Fig. 2. Micromorphological and microstructural characteristics of shallow to deep-water and transplanted morphotypes of *S. pistillata* scleractinian coral. (A) Distal views of individual corallites from colonies collected along the depth gradient. All corallites show organization typical of *S. pistillata* clade 4 (COI molecular phylogeny). (B) The coenosteal spines in shallow-water forms have a larger area of granular texture (red-transparent) than the deeper-water ones (blue-transparent zones mark the smoother zone of the spine). The granulae correspond to Rapid Accretion Deposits (RAD) thus their more extensive development in shallow-water forms points to higher growth dynamics of those skeletal parts. RAD's are clearly visible also in thin-sectioned coenosteal spines of shallow-water morphotypes (C, yellow arrows) which are longer in comparison to deeper-water forms (C). Transplanted morphotypes develop coenosteal spines that show shallow-water and deeper-water characteristics (60 to 5 m and 5 to 60 m, respectively). A, B, Scanning Electron Microscopy images; C, Transmitted optical microscopy images (polarized light). (For interpretation of the references to color in this figure legend, the reader is referred to the web version of this article.)

Calcification (CoC) [23]. Consequently, their more extensive development in shallow-water forms points to increased growth dynamics of those skeletal parts.

The micro-CT longitudinal sections of branches of coral colonies originated in shallow-water (5 m and transplanted from 5 m to 60 m) show lighter skeletal structures with numerous larger and

closely packed corallites with thicker septa that form a fan-like pattern; dissepiments (domed skeletal plates within corallites) in those morphotypes are not regularly distributed (Fig. 5A, movies S1-S4). Conversely, the corals that originated in mesophotic depths (60 and transplanted from  $60 \rightarrow 5$  m) are characterized by smaller corallites situated further apart with a dense skeleton at the

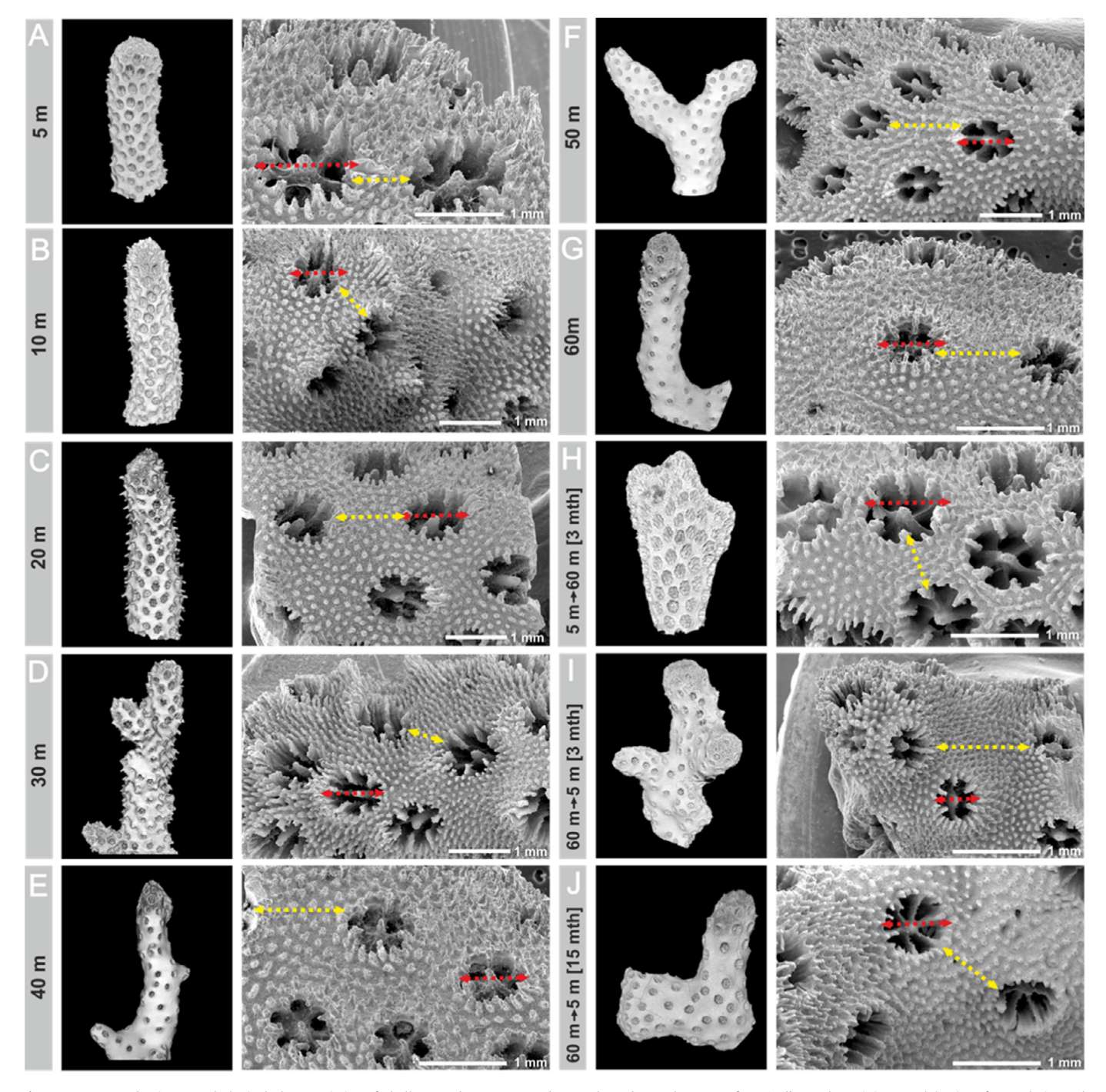


Fig. 3. Macro- and micromorphological characteristics of shallow to deep-water and transplanted morphotypes of *S. pistillata* scleractinian coral (A-J). Left panels in each column show the distribution of corallites on colony branches (micro-CT imaging). Right panels show SEM micrographs of the corallite (red arrow) and coenosteum development between the corallites (yellow arrow). (For interpretation of the references to color in this figure legend, the reader is referred to the web version of this article.)

branch perimeter and they have regular dissepimental layers with thinner septa in the central region of the branch. Virtual transverse sections made 5 mm from the branch tip show that morphotypes originated in shallow-water (5 m and transplanted from 5  $\rightarrow$  60 m) develop closely-packed and denser corallites, whereas the morphotypes originated in mesophotic depths (60 m and transplanted from 60  $\rightarrow$  5 m) have larger coenosteal area (lesser corallite density), more porous inner but thickened outer parts of the branch (Fig. 5B). Moreover, comparing the porosity of the inner part of the branch (Fig. 5B), we found that these values show a clear shift between the corals from the original location and the

transplanted ones. The original inner-branch porosity is higher by 17% in the 60 m morphotypes compared to 5 m ones. The porosity of the transplanted coral slowly shifts off their original value, the porosity of the transplanted corals from 5 m to 60 m increased by 3% from the control 5 m morphotypes whereas inner-branch porosity of corals transplanted from 60 m to 5 m decreased by 5% and 8% during 3 and 15 months after reciprocal transplantation, respectively, compared to the control 60 m morphotypes.

Changes in the skeleton morphology were complemented by a change in the crystallite size of the mineral as indicated by highresolution synchrotron X-ray powder diffraction (HRPXRD) mea-

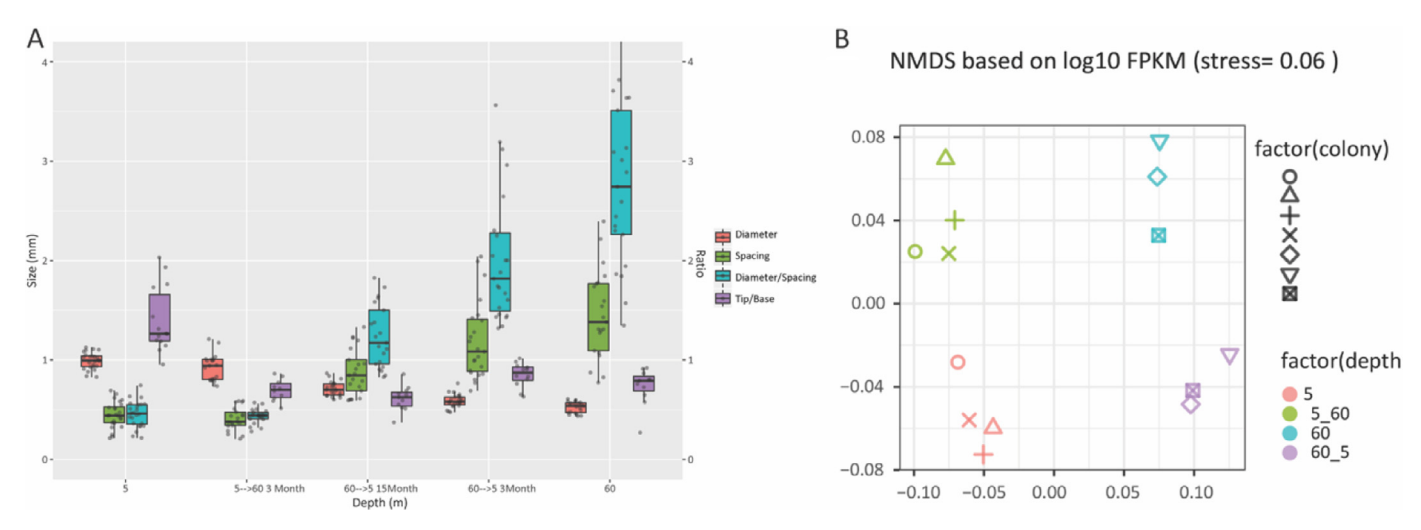
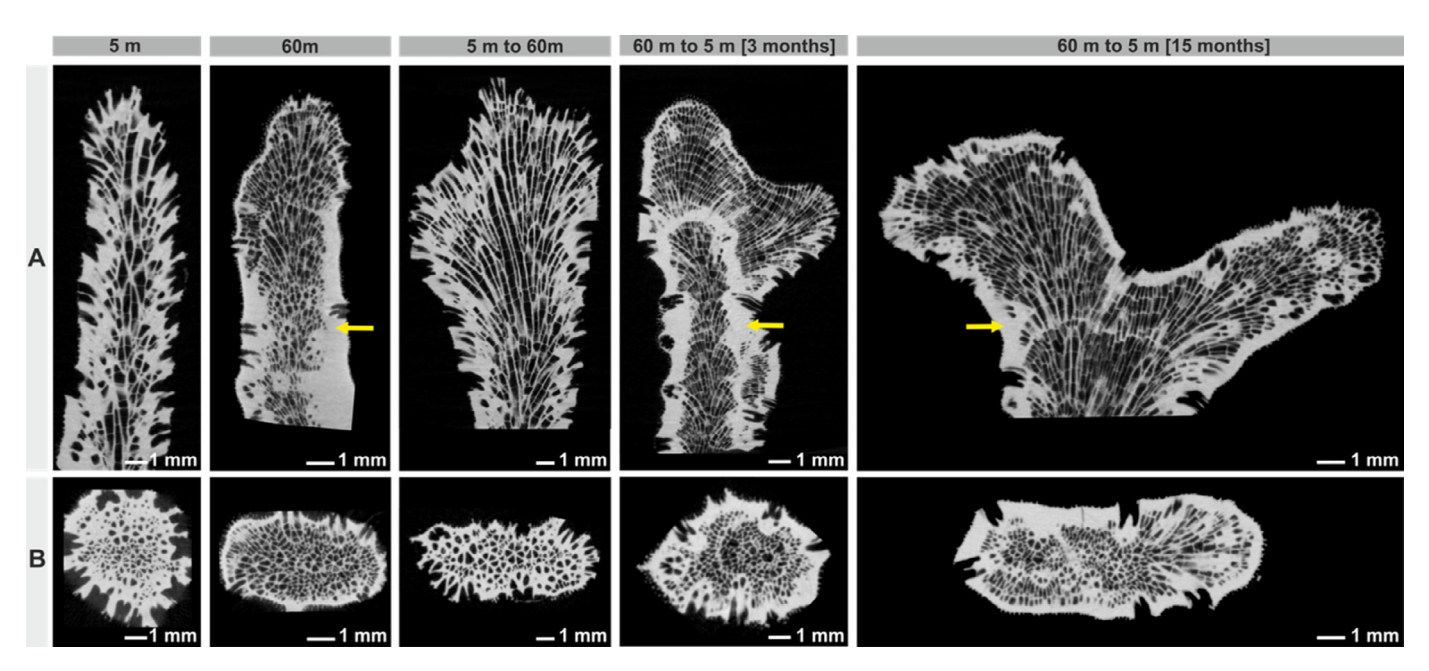


Fig. 4. Morphological and gene regulation differences after reciprocal transplantation (A) Changes in corallite diameter (red), corallite spacing (green), the ratio of diameter to spacing (cyan) and the ratio of coenosteal spines tip (RAD) to base (purple) after transplantation. Mann–Whitney–Wilcoxon p values between these groups of samples are shown in Table S1 and indicate a significant environmental effect. (B) similarity between samples using Non Metric Multidimensional Scaling (NMDS) ordination, based on Bray-Curtis distances calculated from log10 the samples' FPKM values (fragments per kilobase per million mapped RNA-Seq fragments), of untreated vs. transplanted samples. NMDS Stress of 0.06 indicates a good fit. (For interpretation of the references to color in this figure legend, the reader is referred to the web version of this article.)



**Fig. 5.** Micro-CT virtual sections of colony branches of *S. pistillata* shallow to deep-water and transplanted morphotypes. (A) Longitudinal sections of corals originated from shallow-water (5 m and transplanted from 5 m to 60 m) show lighter skeletal structures with numerous and closely packed corallites forming a fan-like pattern; dissepiments are not regularly distributed. Conversely, morphotypes originated from deep-water (60 m and transplanted from 60 m to 5 m) form dense skeleton at branch perimeter (yellow arrows) and show regular dissepimental layers in less dense central region of the branch. (B) Transverse sections made ca. 0.5 mm from the branch tip. Morphotypes originated from shallow-water (5 m and transplanted from 5 m to 60 m) show numerous corallites (high corallite density) and generally a thicker skeleton, whereas morphotypes originated from deep-water (60 m and transplanted from 60 m to 5 m) show lesser corallite density, more porous central and thickened outer part of the branch. (For interpretation of the references to color in this figure legend, the reader is referred to the web version of this article.)

surements. Even though diffraction patterns collected from all the studied corals have been well indexed to be aragonitic (Fig. S2), the shallow water corals exhibit broader diffraction peaks, suggesting smaller crystallite sizes, as compared to those of the mesophotic depths colonies (Fig. 6A). For the synchrotron XRD patters, each diffraction peak shape has the contribution of Lorenzian and Gaussian functions, where the Lorenzian is related to crystallite size and the Gaussian to micro-strain fluctuations. Deconvolution of the diffraction peak shape makes it possible to determine the contribution of each function separately and is useful to estimate crystallite sizes and micro-strain fluctuations along specific crys-

tallographic reflections. Utilizing line profile analysis [24,25], the crystallite sizes along the (111), (012) and (200) aragonite reflections were calculated for the shallow- and deep-water corals to be 266 $\pm$ 3 and 379 $\pm$ 4 nm, 218 $\pm$ 2 and 314 $\pm$ 5 nm, and 190 $\pm$ 31 and 262 $\pm$ 6 nm, respectively. Moreover, the transplanted corals demonstrate a clear change in sizes towards that of the reciprocal transplantation site. Thus, the crystallite size of the transplanted 5  $\rightarrow$  60 m corals increased, while transplanted 60 to 5 m specimens showed a decrease in the crystallite size (see crystallite size prior to heating in Fig. 6B). In addition, the organic matrix of the skeleton increases as the porosity increase at the deep corals. To test

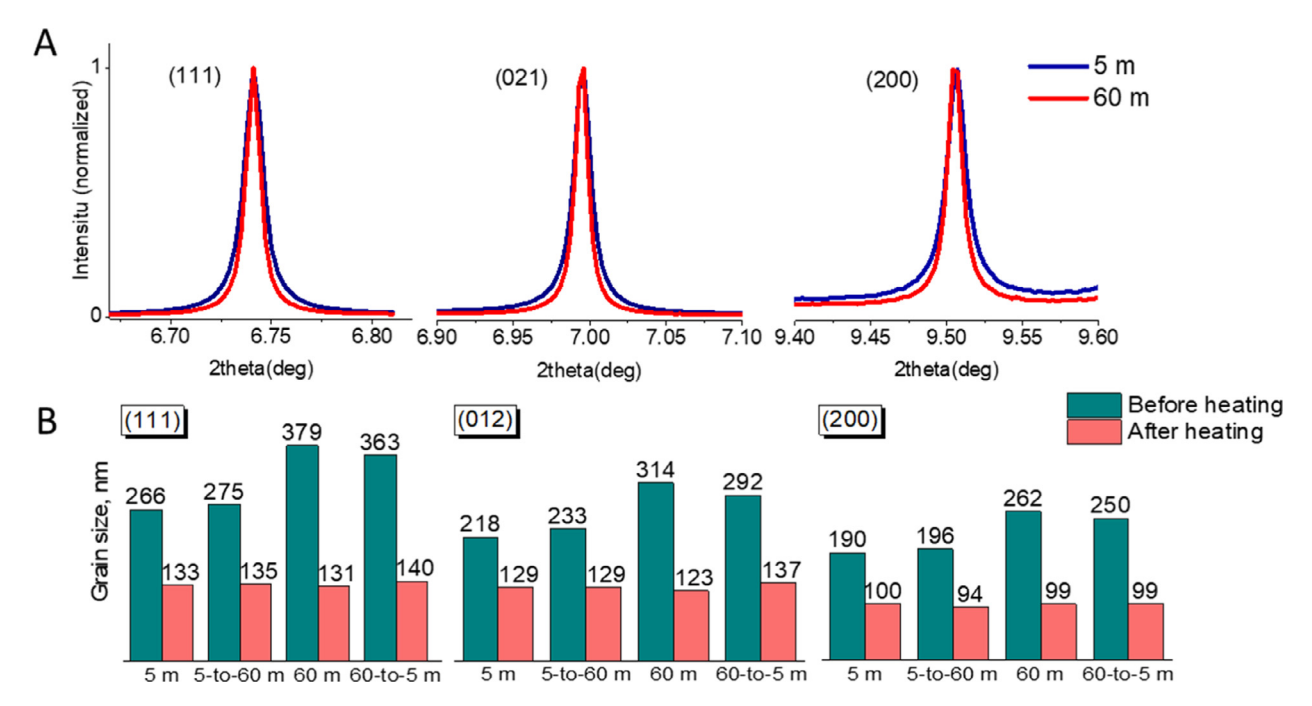


**Fig. 6.** XRD analysis of the shallow-, deeper-water and transplanted corals. (A) (111), (021) and (200) diffraction peaks of the 5 and 60 m corals demonstrating a clear broadening of the diffraction peaks of the shallow-water corals relative to the deeper-water colonies. Diffraction patterns are collected at a wavelength of 0.4 Å. (B) Calculated crystallite sizes along (111), (012) and (200) crystallographic directions for shallow-water (5 m and 5 to 60 m) and deeper-water (60 m and 60 to 5 m) species before and after ex-situ heating at 300 °C for 2 h. (For interpretation of the references to color in this figure legend, the reader is referred to the web version of this article.)

the influence of the organics on the mineral, we preformed ex-situ heat treatment prior the HRPXRD measurements. We found that after ex-situ heat treatment the crystallite size of the 60 m corals decreases almost 3-fold, while for the 5 m corals it is not more than twice as low as prior to annealing (see crystallite size after heating in Fig. 6B). The latter implies that a higher amount of organic material decomposed upon annealing within the deep-water minerals.

In order to identify the molecular mechanisms associated with the changes in fine-scale and crystallographic skeletal features across the depth-gradient and in transplanted colonies, genetic analysis was performed in an attempt to identify a group of genes which may underline the above phenotypic plasticity.

# 2.2. Phenotypic vs. transcriptomic changes between shallow and mesophotic depths

The molecular basis underlying depth-specific morphology differences was assessed by testing gene expression control in *S. pistillata* samples at various depth points (5, 10, 30, 50, and 60 m), using RNA-Seq. Overall, the comparison of mesophotic (50–60 m) vs. shallow (5–10 m) samples shows an upregulation vs. downregulation of 20% vs. 19% of 24,604 transcribed *S. pistillata* genes (Tables S2). Comparisons between groups of samples taken from adjacent depth-points gave significantly lower counts of differentially expressed (DE) genes.

The downregulated group (higher at shallow water) is significantly enriched with genes known to be associated with the control of oxygen metabolism, including mitochondrial respiratory chains activity, NADP/FAD binding, ATP-dependent chromatin remodeling, etc. Oxidative stress response genes, including DNA-repair genes, were also significantly enriched (Fig. 7; Tables S3 and S4).

The upregulated group (higher at mesophotic depths) was significantly enriched with genes known to be associated with the

control of cilia formation, and numerous developmental processes including neural development, likely reflecting the switch to predation activity as a primary source of energy at depth (Fig. 7; Tables S3 and S4). In addition, among 39 known as "tool kit" biomineralization genes in *S. pistillata* [26], 15 genes were significantly upregulated and only 3 were downregulated between mesophotic and shallow water, a difference which is significant (*p*-value <0.05) using Sign Test (Table S5).

# 2.3. Transcriptome plasticity and adaptation to depth as a result of reciprocal transplantation

The effect of reciprocal transplantation on gene expression was tested on transplanted colonies from 60 m to 5 m, and from 5 m to 60 m using RNA-Seq, after 3 months at the new depth (Table S6). As shown in Fig. 7 heatmap, large groups of genes from transplanted samples adapted the patterns typical to the new depth (namely  $60 \rightarrow 5$  transcriptome becomes more similar to 5, while  $5 \rightarrow 60$  become mores similar to 60). As shown in Fig. 7 bottom panel, the transcriptomes of the transplanted group of samples have gained functional patterns typical to the destination depth (and see also Tables S3, S4, and S7).

# 2.4. Environmental and colony effect on transcriptomic response after transplantation

In total, ~40% of all genes were differentially expressed between shallow vs. mesophotic depths (regardless of reciprocal transplantation), compared to ~12% and ~25% as a result of the reciprocal transplantation to 5 m and to 60 m, respectively. This means that original expression patterns are partly maintained for months after the reciprocal transplantation. Accordingly, as NMDS ordination shows (Fig 4B), expression patterns of transplanted samples are affected by both the colony factor (reflecting genetics, epigenetics, physiology) and the environmental factor (reflecting abiotic/biotic conditions associated with depth).

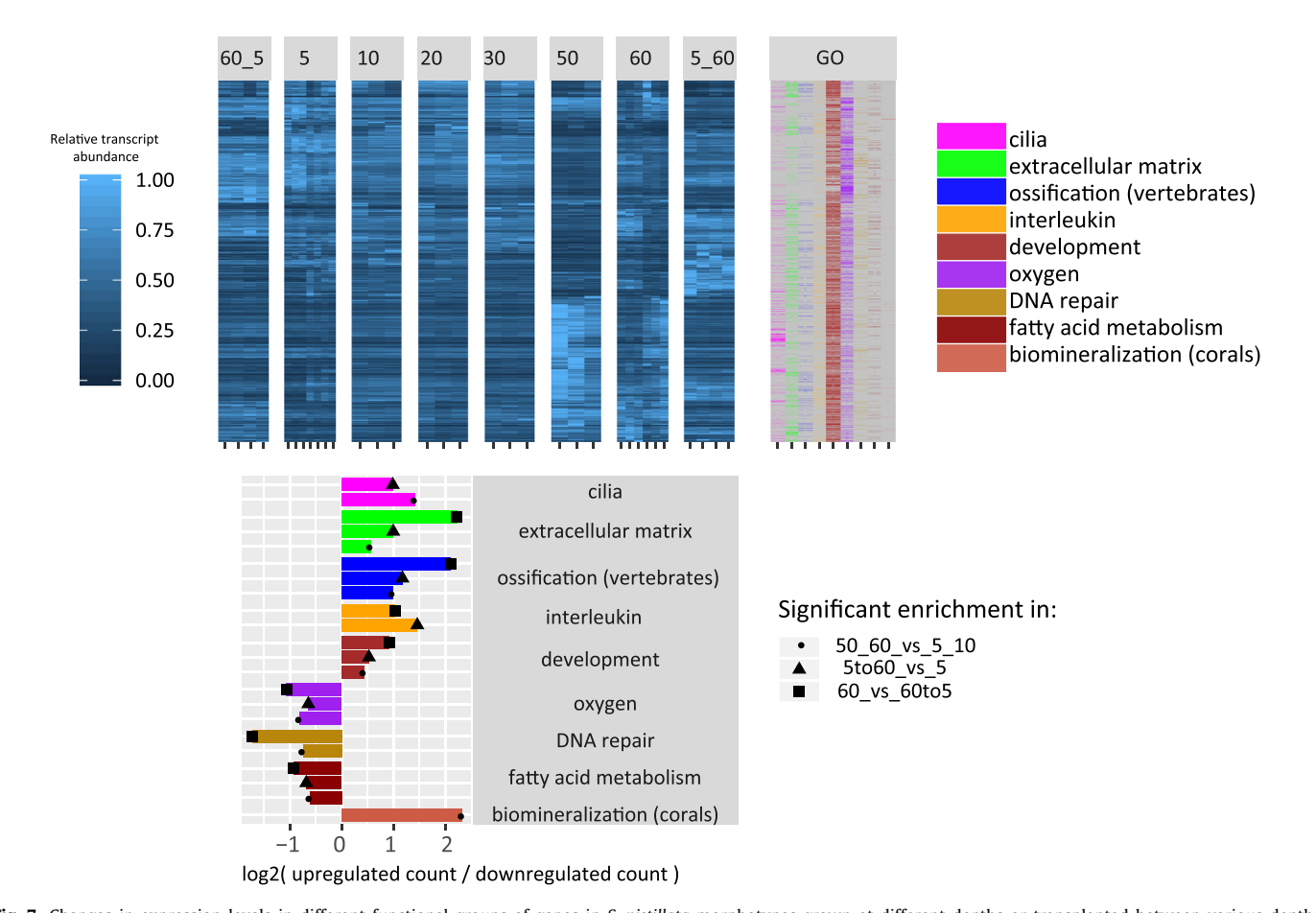


Fig. 7. Changes in expression levels in different functional groups of genes in *S. pistillata* morphotypes grown at different depths or transplanted between various depths. Upper left: a heatmap of transcripts relative abundance (as the fraction of the maximum FPKM per gene) (percentile), where the " $60 \rightarrow 5$ " and " $5 \rightarrow 60$ " groups represent samples transplanted from 60 m to 5 m and from 5 m to 60 m, respectively. The heatmap represents genes belonging to specific functional groups, that are significantly differentially expressed in the shallow-water vs. deep-water groups, and/or after transplantation; Upper right: a heatmap of biological functions associated with the genes from the left heat map. The group "coral biomineralization" includes genes known to be involved in this process in corals. Other groups represent subgroups of functionally related GO terms, for example: the term "oxygen" represent the terms "mitochondria", "oxidative-stress", "oxidoreductase", etc. Similarly, the "DNA repair" group includes "mismatch repair", "response to UV", etc. Bottom: the horizontal bars show the  $\log_2$  of the count of significantly upregulated divided by significantly downregulated genes, for specific depth comparisons and functional groups. The bars are shown only for cases with significant (p value < 0.05) enrichment of upregulated vs. downregulated genes, based on Sign Test. (For interpretation of the references to color in this figure legend, the reader is referred to the web version of this article.)

# 2.5. Biomineralization-related genes

Biomineralization "tool kit" genes [26,27], found to be expressed here (Table S5), encode proteins containing one or more transmembrane domains, extracellular matrix proteins, and collagen. Out of thirty-eight expressed tool kit genes, fifteen were significantly upregulated in the deep vs. shallow water, and only three were downregulated (enrichment p-value=0.0075 using Sign-test). Most of these differentially expressed biomineralization genes are known to play a role in promoting extracellular matrix, attachment of the calicoblastic cells to the skeleton, adhesion glycoproteins, collagen, and carbonic anhydrase (STPCA2). Similarly,  $SLC_4\gamma$ , which was suggested to be a coral-specific transporter of bicarbonate ions to the site of calcification [28], was significantly upregulated in 60 vs. 5. In contrast,  $SLC_{4\beta}$  which is a putative  $SLC_4\gamma$  paralog but not a coral-specific gene [28], was among the three biomineralization-related genes downregulated in deep water (Fig. S4A, Table S6). The coral biomineralization gene CARP1 [29] showed no 60 vs. 5 change but was significantly downregulated in both 60 vs.  $60\rightarrow 5$ , and  $5\rightarrow 60$  vs. 5 comparisons.

We identified 59 acidic proteins candidates, from which 2 were found to be basic, based on their isoelectric point, and secretion peptides were found only at 14 proteins. We further tested the expression of these 59 genes (contains >30% aspartic and glu-

tamic acid; Table S8), due to the potential involvement of this group in biomineralization. We found no enrichment of acidic genes among down- or up-regulated genes between shallow and mesophotic depths (Table S8). These results corroborate the observation of no enrichment of acidic amino acids in the coral skeletal organic matrix between 5 vs 60 m as measured by GC-MS (Fig. S5). The identity of differentially expressed acidic genes differ between the different comparisons (transplanted vs. control, shallow vs. mesophotic), although the proportion of up- and downregulated genes remain comparable.

# 3. Discussion

Phenotypic plasticity, which we identify as the ability to develop different environmental-induced phenotypes during the life of single organisms [30], facilitates diversification and speciation during evolution. Our phylogenetic analysis revealed that although the colony structure and the micro-scale skeletal features vary throughout shallow to meshophotic depths, all corals examined were clearly identified as belonging to *S. pistillata* clade 4 [22].

The reciprocal transplantation results indicate that within 3 months, samples moved from mesophotic depths to shallow waters, or from shallow to mesophotic depths, partly adapted both morphological-characteristics and transcriptomic functions typical

to corals in their destination environments. The adaptation rate is gradual, and the transplanted corals become more and more similar to coral found in their destination environment with increasing exposure from 3 to 15 months, as evidenced by both our morphological and gene expression patterns (Fig. 4).

At the transcriptome level,  $60 \rightarrow 5$  m corals drastically change their function toward increased control of oxidative phosphorylation, oxidative stress response, DNA-repair, apoptosis, and the accessibility of the repair machinery to the DNA via ATP-dependent chromatin remodeling [31]. Overall, these results correlate with increased symbiont photosynthesis which leads to elevated oxidative stress associated with higher glucose metabolism, respiration, and hyperoxia. Indeed, in shallow water photosynthesis rates are known to be elevated in coral symbionts [18,32]. Additionally, photosynthesis of coral symbionts was suggested to be associated with host hyperoxia during the day, yet nearly hypoxic conditions at night, where both conditions can lead to elevated levels of Reactive Oxygen Species (ROS) and cellular damage risks [33]. In 2015, Cohen et al. [32] tested physiological parameters of S. pistillata corals responding to reciprocal transplantation from 3 m to 30 m and vice versa. They found that the respiration of S. pistillata was more than twice the rate at 3 m than at 30 m, and that respiration is increased with shallow reciprocal transplantation while decreased with deep one. On the other hand,  $5 \rightarrow 60$  m corals increase transcriptomic control functions associated with numerous developmental-related processes, including biomineralization toolkit genes, regulation of extracellular matrix interactions, and presumably neural control of predation activity - which become critical in mesophotic environments [14].

Accompanying the transcriptomic observations, all examined colonies show phenotypic plasticity along the depth gradient. It affects colony structure and various macro-and micro-scale and crystallographic skeletal features. The shallow-water morphotypes form spherical colonies whereas deeper-water morphologies are flatter. Similar to previous observation [14] we found that the calicular diameters of the corallite decrease with depth while the distances between calices, or coenosteal area is smaller in shallowwater. The coenosteal spines in shallow-water forms have a larger area of granular texture (corresponding to the development of RAD's) than the deeper-water ones. Interestingly, the reciprocal transplant results support the previous finding by showing rapid phenotypic plasticity in response to environmental changes. After 3 and 15 months of reciprocal transplantation, the colonies began to show skeletal characteristics typical of the new location. For example, the granular texture of coenosteal spines (Fig. 2B), the length of the spine (Fig. 2C) and the porosity (Fig. 5) after a reciprocal transplantation shift toward those of the morphotypes in the target environment. Additionally, the crystallite size and the organic matrix composition as measured by HRPXRD shift toward the reciprocal transplantation site. An increased porosity and increase of skeleton organic matrix were typical for the mesophotic colonies. Similar observations were reported for corals grown under seawater acidification conditions [34], were calcification rates are slower. Tambutte et al. [34] suggested that the corals may increase levels of skeleton organic matrix proteins to promote calcification under less favorable calcifying conditions. We assume that the increased porosity of the skeleton of S. pistillata and other morphological change in coralla of S. pistillata (Fig. 5) may be explained by lower calcification rates that actually were reported for the corals from mesophotic depths [18]. The ecological consequences of developing a more porous inner part with a dense skeleton at the branch perimeter are unknown, but it can be speculated that this is a useful strategy to enhance light scattering. Increasing light scattering within the coral skeleton explains increased light absorption efficiency of the coral symbionts [35]. Variation in the ability of the skeleton nano-to-micro-scale structures to influence the light path has been previously documented [36]. Thus, the optical properties of coral skeletons may have a direct impact on the holobiont photosynthetic performance. Since extracellular matrix proteins play a crucial role in the skeletal formation of corals, particularly interesting was a comparison of abundances of transcripts encoding biomineralization "tool kit" proteins [26]. Overall, among twenty-nine differentially expressed tool-kit genes (in either: 60 vs 5, 60 vs 10, 50 vs 5, 50 vs 10; Table S5), twenty-four were upregulated in mesophotic colonies, and only five were downregulated - a statistically significant difference. Interestingly, most of these differentially expressed transcripts encode proteins that play a role in the structural, adhesive and metallo-proteins activity. These enable cell-cell and cell-substrate adhesion and modify the calcifying environment [26,37]. Yet, among these biomineralization proteins, those harboring acidic residues (e.g. CARPs) which catalyze the nucleation of the biominerals [29], did not show clear depthdependent trends of expression.

Our search for proteins with more than 30% aspartic and glutamic acids also revealed fifty-nine such genes, and among them seven were downregulated and nine were upregulated in shallow vs. mesophotic, indicating no depth-dependent trend. In addition, we did not observe significant differences of amino acid composition between the up- and down-regulated acidic genes. This corroborates the hypothesis that acidic proteins play a major role in coral skeleton formation [38] and although mesophotic corals calcification rates are lower, [18] the basic mineralization mechanisms remain the same.

The fact that after reciprocal transplantation, the *S. pistillata* biomineralization acidic genes CARPs 1 and CARP3 were upregulated at shallow depth, may reflect their role in nucleation. Since CARP1 was found to be localized around CoC/RAD [39], after reciprocal transplantation from mesophotic to a shallow depth, the formation of the fine-scale granulae on coeanosteal spines, which correspond to CoC/RAD increase, may be associated with the upregulation of CARP1 and its effect on RAD formation.

We observed that S. pistillata carbonic anhydrase (STPCA), bicarbonate transporter (SpiSLC4 $\gamma$ ) and collagen were among the upregulated genes in corals from mesophotic depths. Previous works showed that STPCA is localized at the calicoblastic ectoderm level [37,39] and in the skeletal organic matrix of the coral [26]. This enzyme was found to be involved in Ca<sup>2+</sup> deposition [40] and the inhibition of STPCA caused rates of calcification to be up to 50% lower [37]. In this research, STPCA was upregulated in the mesophotic corals. Overexpression of STPCA in the mesophotic zone might be linked to the finding that STPCA is upregulated at night in order to deal with night acidosis [37] (even though calcification rates at night are low) by hydrating CO<sub>2</sub> into bicarbonate, producing 2H<sup>+</sup>, which are then exchanged with a Ca<sup>+2</sup> ATPase exchanger for one Ca<sup>+2</sup>. The decrease in photosynthesis rates with depth [18] may lead to increasing levels of CO2 with depth, leading to acidosis, resulting in upregulation of STPCA. The carbonic anhydrases mediate the subsequent carbonate chemistry necessary in the deep corals where photosynthesis rates are low [12] which can lead to low carbonate concentration.

Another biomineralization tool-kit gene which was upregulated in the mesophotic environment is SpiSLC4 $\gamma$ . Orthologs of SpiSLC4 $\gamma$  exist only in robust and complex clades of scleractinians [41], and it was suggested that they are involved in the calcification process. It was suggested that SLC4 proteins can bind coupled to a cytoplasmic carbonic anhydrase, such as STPCA2, and accelerate transmembrane bicarbonate transport to the site of calcification [28].

Our study has several broader ramifications for understanding the coral plasticity under gradually changing environmental parameters and for the scleractinian evolution and their fossil record. The current concern regarding climate change i.e.,

global warming and ocean acidification, is the greatest threat to coral reef ecosystems. As most of the reef corals operate near their upper limit of heat tolerance [42], mass bleaching (disruption of relationships with symbiotic algae) occurs when the surface waters become too warm, well above their normal summer temperature. Additionally, the current rate of CO<sub>2</sub> increase in the atmosphere is overwhelming Earths capacity to buffer the ocean [43] and the carbon dioxide absorbed into the ocean from the atmosphere contributes to changes in calcification rates of corals. All these climate-related factors favor migration to deeper water settings (mesophotic depths). This may emerge as a successful evolutionary strategy for some reef-coral species. From a deeptime (Paleozoic-Cenozoic) evolutionary perspective, scleractinian diversity survived several bottleneck phases during oceanic chemical/physical changes and deep-water refugia most likely were the major sources of revitalization of the group [44,45]. Moreover, the comprehensive molecular phylogenies based on large azooxanthellate and zooxanthellate scleractinian taxa molecular datasets suggest that the oldest scleractinian lineages were azooxanthellate and solitary and that the order probably had shallow-water origins but later "invaded" deep-water environments [46,47]. All this evidence suggests that coral migration from shallow to deep-water and vice versa were common evolutionary strategies. Understanding the molecular, physiological and biomineralization effects of these migration processes that provide our study will allow prediction of possible responses to migratory pressure of other corals living along the depth gradients.

#### 4. Methods

#### 4.1. Sample collection

Colonies of the hermatypic coral *S. pistillata* (Esper, 1797) were collected under a special permit by the Israel Nature and Parks Authority, from a depth gradient ranging from 5 m to 60 m every 5 m, in front of the Interuniversity Institute for Marine Science (IUI) at the Gulf of Eilat, in the northern Red Sea (29° 30′ N, 34° 56′ E). Deep dives were accomplished using Megalodon closed circuit rebreathers (Innerspace Systems) as well as NITROX and Trimix SCUBA.

## 4.2. Reciprocal transplantation

We transplanted five coral colonies from 5 to 60 m (5  $\rightarrow$  60 m) and from 60 to 5 m (60  $\rightarrow$  5 m) following the protocol describe by (Cohen et al. 2015). Briefly, five coral colonies from 5 to 60 m (ten colonies in total) were fragmented into twenty-five fragments. Twenty-four of them were returned to the sea for reciprocal transplantation after Alizarin red staining, which will allow the differentiation between old skeleton (before reciprocal transplantation) and new skeleton (after reciprocal transplantation). Twelve fragments from each colony served as the control group and were hung from a large  $(1 \times 2 \text{ m}^2)$  table at their original depth. The other twelve were the treatment group and hung from a small  $(1 \times 1 \text{ m}^2)$  table. The fragments on the small table were transplanted over a course of three months and six stations to their final destination, where they were placed on the large table with the control fragments. Unfortunately, all the colonies at the 60 m table were covered by tunicate and died after 5 months while the  $60 \rightarrow 5$  m colonies kept growing for another 12 months. After three months three colonies control and transplanted colonies were sampled while the rest of the colonies remained. The samples were collected for phylogenetic analysis, micro-CT imaging, SEM and cross polarization imaging, X-ray and RNAseq as described below, in order to reveal whether the differences between shallow reef corals and mesophotic reef corals are mediated through intrinsic or extrinsic factors.

#### 4.3. Phylogenetic analysis

Triplicate samples from each depth (5 m, 10 m, 15 m, 20 m, 25 m, 30 m, 40 m, 50 m and 60 m) and one branch of each of the transplanted corals were preserved in 70% (v/w) ethanol and frozen at -20 °C prior to DNA extraction. DNA was extracted using a Promega Wizard® Genomic DNA Purification Kit, follow the manufacture's protocol with a slight modification. In brief, small fragments were placed in 1.5 ml of the manufacturer's lysis buffer and 55ul Proteinase K, followed by an overnight incubation at 55 °C, then 750 µl of the resulting liquid was used to continue the manufacturer's protocol. Polymerase Chain Reaction (PCR) was performed for the COI region using primers LCO1490: 5'-ggtcaacaaatcataaagatattgg-3' and HC02198: 5'-taaacttcagggtgaccaaaaatca-3' as described in [22]. PCR products were analyzed on a 1% agarose gel electrophoresis, cleaned using Promega Wizard® SV Gel and PCR Clean-Up System following manufacturer protocol and sequenced in the Sanger sequencing method using the ABI 3730xl DNA Analyzer. Sequences were aligned and a phylogenetic tree was generated using MEGA7© software and compared to the database generated by [22]. The evolutionary history was inferred by using the Maximum Likelihood method based on the Hasegawa-Kishino-Yano model [48]. The tree with the highest log likelihood (-860.59) is shown. The percentage of trees in which the associated taxa clustered together is shown next to the branches. Initial tree(s) for the heuristic search were obtained automatically by applying Neighbor-Join and BioNJ algorithms to a matrix of pairwise distances estimated using the Maximum Composite Likelihood (MCL) approach, and then selecting the topology with superior log likelihood value. The tree is drawn to scale, with branch lengths measured in the number of substitutions per site. The analysis involved 37 nucleotide sequences. Codon positions included were 1st+2nd+3rd+Noncoding. All positions containing gaps and missing data were eliminated. There was a total of 533 positions in the final dataset. Evolutionary analyses were conducted in MEGA7 [49].

# 4.4. Micromorphological and microstructural analyses

The coral fragments were placed in distilled water post collection for 24 h, after which, the tissue was removed, using an airbrush, and then dried in an oven at 60 °C overnight. The samples were cut into ca. 1 cm pieces, mounted on the stubs and sputtercoated with conductive platinum film. Skeletal micromorphological features were visualized with Philips/FEI XL20 Scanning Electron Microscopy. The skeletal fragments not used for SEM were thin-sectioned. Ca. 15 µm thin petrographic sections were observed and photographed with a Nikon Eclipse 80i transmitted light microscope fitted with a DS-5Mc cooled camera head. Observations conducted in polarized light provide some preliminary information about the crystallographic organization of aragonite fibers: identical interference colors or complete light extinction indicate similar arrangement of axes of individual crystallographic domains. In addition, fragment of each colony was imaged in 3D (9 µm pixel size, 360 deg, 70 keV) by laboratory micro CT (Skyscan 1275, Bruker micro CT, Kontich - Belgium). Following reconstruction (NRecon 1.7, Bruker micro CT, Kontich - Belgium) the full architecture of the corals was examined in both 2D and 3D (ImageJ 1.52d, National Institutes of Health, USA; CTvox, Bruker micro CT, Kontich, Belgium).

The corallite diameter and the minimum distance to the nearest neighbor were imaged with a Nikon dissecting scope and measured with ImageJ software [50] from 3 arbitrary images taken at a distance of 2 cm from the terminal branch end of 3 colonies of

each treatment (N=20–26). The ImageJ software [50] was also used to assess the coenosteal spines tip (with clearly visible granular texture (RAD)) to base ratio. Measurements of at least 20 spines (N=21–29) from approximately the same colony region (middle part of the colony branch) were done using SEM images. The ratio was taken between length of the area with granular texture (red-transparent in Fig. 2) to length of smoother zone of the spine (blue-transparent zone in Fig. 2). Both measurements were taken along the spine axis.

### 4.4.1. Statistics of morphological data

We compared groups of measurements using Wilcoxon rank sum in R (Wilcox test where paired=FALSE).

## 4.5. High-resolution powder X-Ray diffraction

These measurements were conducted at beamline ID22 of the European Synchrotron Radiation Facility (ESRF, Grenoble, France) at a wavelength of 0.4 Å. This beam line uses a highly collimated and monochromatic beam to perform powder diffraction in the Laue setting. The beam passes through the sample and diffracts, to be collected on the opposite side by a set of 9 synchronized detectors, mounted 2.2° apart. The intensity of the diffractions is integrated over all detectors to produce high-resolution diffraction patterns. Instrument calibration and wavelength refinement have been performed with silicon standard NIST 640c.

The coral samples were air-dried and grounded to a fine powder using an agate mortar and pestle. Powdered samples were loaded into borosilicate glass capillaries of diameter 0.7–1 mm. Measurements were performed at room temperature for the corals as collected and after ex-situ heating at 300 °C for 2 h. Coherence length (nm) along various crystallographic directions was derived applying the line profile analysis to a specific diffraction peak. This was carried out by fitting the profile to a Voigt function and deconvoluting the Lorenzian and Gaussian widths as described in [24].

### 4.6. Skeleton amino acid composition

A total of 1 g homogenized coral skeleton powder (smaller than 63 µm) was bleached and placed in an 18 cm cellusep® T1 dialysis bag. 20 mL of double distilled water was added to the bag and sealed tight with plastic clips. The dialysis bags were placed in a glass beaker with 2 L of acetic acid 0.1 M at 4°C on a magnetic stirrer. Samples were left in dialysis solution until a complete decalcification of the sample. The dialysis medium was changed every 24 h. At complete decalcification, dialysis medium was changed to double distilled water to a neutral pH. Dialysis bag content was placed in a 50 mL corning falcon tube and lyophilized. The dry sample was then hydrolyzed using 2 mL HCL 6 N at 150°C for 70 min, under N<sub>2</sub> atmosphere, inside 4 mL glass vial with PTFE cap [51]. Under these conditions cysteine and tryptophan are destroyed, glutamine transforms to glutamic acid and asparagine to aspartic acid. Samples were left on bench to cool to room temperature. The sample was sieved through a 0.22µ PTFE filter to remove all undissolved particles. Sample was evaporated at 70°C under a gentle stream of N<sub>2</sub>. Derivatization of acid hydrolyzed sampled carried out using the EZfast® amino acid analysis kit with slight modification of replacing reagent number 6 with dichloromethane as a solvent. 1.5 µL of sample was injected in splitless mode with inlet temperature of 250 °C, Helium was used as a carrier gas at constant flow of 1.5 ml/min. The amino acids were separated on a Zebron ZB-50 column (25 m, 0.25 mm and 0.25 µm) in Thermo Scientific Trace 1300 Gas chromatography GC. The GC condition was set to optimized peak separation for the desired amino acids as follows: Initial temperature of 110 °C and then ramped to 320 °C at 8 °C per minute and held for 2.5 min. The separated amino acids run through Thermo Scientific ISQ mass Spectrometer and the conditions were set to: transfer line 310 °C, ion source 240 °C and scan range from mass 43 to 450 m/z.

#### 4.7. RNA extraction, processing and sequencing

Triplicate samples from each depth were collected at May 2017 (5 m, 10 m, 20 m, 30 m, 50 m and 60 m) and after 3 month of reciprocal transplantation at July 2018 (5 m, 5>>60 m, 60 m, 60>> 5 m) were placed in 1.5 ml tubes containing 700 μl TRI Reagent<sup>TM</sup> Solution (Ambion<sup>TM</sup>), snapped frozen in liquid nitrogen and kept at -80 °C prior to RNA extraction. Total RNA was extracted using TRI-Reagent (Sigma) following the manufacturer's protocol with some modification. Briefly, for RNA lysis and homogenization samples were defrosted at 37 °C and transferred (liquid and fragment) to a QIAGEN© QiaShreader cartridge and centrifuge at top speed for 1 min and liquid was transferred to a different tube. An extra TRI Reagent<sup>TM</sup> were added to the collection tube to bring the volume up to 1 ml, 100 µl 1-bromo-3-chloropropane was added, and the solution was than vortexed, incubated at room temperature for 10 min and centrifuge at 12,000g for 15 min. Supernatant was transferred to a new sterile 1.5 ml tube. Next, binding, washing and eluting was done using PureLink® RNA Mini Kit (Invitrogen<sup>TM</sup> Ambion<sup>TM</sup>) following manufacturer protocol. Extracted RNA quality and quantity was measured using NanoDrop 2000/2000c UVvis (ThermoFisher©) and tested on TapeStation (ThermoFisher©). Three independent samples were generated for each depth.

Libraries were prepared using the Genomics in house protocol for mRNA-seq. Briefly, the polyA fraction (mRNA) was purified from 500 ng of total RNA following by fragmentation and the generation of double-stranded cDNA. Then, end repair, A base addition, adapter ligation and PCR amplification steps were performed. Libraries were evaluated by Qubit (Thermo fisher scientific) and TapeStation (Agilent). Sequencing libraries were constructed with barcodes to allow multiplexing of 2 samples in 2 lanes. Around 973 million single-end 60-bp reads were sequenced per sample on Illumina HiSeq High Output instrument.

# 4.8. Bioinformatics analysis

# 4.8.1. RNA-seq data

For the differential expression (DE) analysis represented here, the following *Stylophora pistillata* datasets were used: (1) depth-gradient experiment SE (Single End) data (NCBI project id PR-JNA594115); (2) reciprocal transplantation experiment SE data (NCBI project id PRJNA594115).

# 4.8.2. RNA-seq quality filtering and mapping

RNA-Seq reads of the above datasets were adapter-trimmed using cutadapt 1.15 (https://cutadapt.readthedocs.io), then low-quality regions were removed with Trimmomatic 0.3 [52], and inspected in Fastqc (www.bioinformatics.babraham.ac.uk). Reads mapped to human genes, NCBI univec databases, and ribosomal RNA databases [53], were filtered out. Illumina reads were mapped to the *Stylophora pistillata* genome assembly (NCBI GCA\_002571385.1) using Star v2.5 [54].

### 4.8.3. Differential expression experimental design

The effect depth on expression, was tested in the following 4 types of comparisons: (1) depths (5 m,10 m, 20 m, 30 m, 50 m, 60 m), from 2017 collection; (2) shallow (5 m,10 m) vs. deep

(50 m,60 m) water, from 2017; (3) 60 m to 5 m reciprocal transplantation vs. 60 m and vs 5 m, from 2018; (4) 5 m to 60 m reciprocal transplantation vs. 5 m and vs 60 m, from 2018. For the reciprocal transplantation experiments, in addition to the depth factor, the colony factor may affect expression levels.

#### 4.8.4. Differential expression analysis

Differential expression analysis was conducted using Bioconductor DEseq2 [55]. Differential expression analysis was conducted separately for the two reciprocal transplantation experiments, where in both cases the combined effect of both the depth and the colony identity was considered as part of the Bioconductor DEseq2 Generalized Linear Model (GLM). For the two depth gradient experiments (2017 experiment), only the depth factor was considered.

# 4.8.5. Functional enrichment analysis using gene ontology classification

Gene Ontology (GO) terms were assigned to Stylophora pistillata predicted proteins and transcripts using Trinotate 3.0.1 (https: //github.com/Trinotate). GO enrichment analysis was conducted in Bioconductor GoSeq [56], using: (1) Wallenius normalization algorithm, which corrects for enrichment biases in count-data; (2) without count-data bias corrections. The results of both options were very similar. As foreground group, all genes analyzed in DE-Seq2 were used, and as a background we used the following subsets: (1) all significant differentially expressed genes; (2) significance at fold change  $\leq \frac{1}{2}$  (log<sub>2</sub>FC  $\leq -1$ ); (3) significance at Fold change  $\geq 2$  (log<sub>2</sub>FC  $\geq 1$ ). We also searched for functional enrichment using the score-based tool Bioconductor fGSEA [57], which implements GSEA algorithm [58]. In fGSEA, log<sub>2</sub>FC values were used as scores. Since terms detected as significantly enriched tend to be functionally related (e.g., the term "base-excision repair" is nested in the term "DNA repair", etc.), we hierarchically clustered terms based on the proportion of genes they share. This allowed classifying all enriched terms into a limited number of functional aggregates.

# 4.8.6. Identification of Stylophora genes candidates for biomineral formation

We obtained genome-based protein databases of the Stylophora pistillata (NCBI GCF\_002571385.1) [59], Acropora digitifera (NCBI GCF\_000222465.1) [60], and Seriatopora sp. [61]. Known biomineral species-specific formation proteins [26,27] were appended to the above protein databases. Orthology relationships between genes of the three species were detected using OrthoFinder v2.2 by first generating orthology-groups (Orthogroups) based on normalized reciprocal best Blast hits' bit scores [62], and then detecting orthologues genes in Orthoroups [63]. Stylophora proteins orthologous (1:1, 1:many, many:many relationships) to known biomineral formation proteins were considered as candidates. In addition, based on prior identification of acidic proteins involved in biomineralization within the organic matrix, we search for acidic sequences containing: (i) high content (more than 30%) of acidic amino acids (Asp-and Glu), (ii) comprising at least 100 amino acid residues and (iii) differentially expressed throughout the depth gradient.

# 4.8.7. Phylogenetics

PCR amplified *Stylophora* Sanger COI sequences were quality filtered and forward/reverse merged using Seqrt, Seqtk and Pear (https://www.ebi.ac.uk) (https://github.com/lh3/seqtk) [64]. *Stylophora* COI sequences from different depth environments, and publically available COI representative sequences, were then

aligned using Mafft [65], gaps were removed with BMGE [66]. Phylogenetic species tree was constructed using Iqtree [67], for 1000 bootstrap replicates (-bb 1000), based on HKY model [68] and Empirical base-frequencies (HKY+F). This model was selected using MedelFinder by finding best fit-model from an initial parsimony tree.

### Acknowledgments

We thank the technical staff of the Moris Kahn Marine Research Station for their invaluable help. We thank Maya Lalzar from the bionformatics Core Unit, University of Haifa, and The Crown Genomics institute of the Nancy and Stephen Grand Israel National Center for Personalized Medicine, Weizmann Institute of Science. The study was performed in accordance with regulations and guidelines set by the Israel Nature and National Park Protection Authority. This research was supported by a Grant from the GIF, the German-Israeli Foundation for Scientific Research and Development and by the Israel Science Foundation (Grant 312/15) to T.M. J.S thanks the funding from National Science centre (Poland) research grant 2017/25/B/ST10/02221.

B.P thanks the funding from the European Research Council under the European Union's Seventh Framework Program (FP/2013–2018)/ERC Grant Agreement No. 336077.

The authors are also indebted to the high-resolution powder diffraction beamline ID22 at the ESRF for the support during the beamline. Computations presented in this work were performed on the Hive computer cluster at the University of Haifa, which is partly funded by ISF grant 2155/15.

### Supplementary materials

Supplementary material associated with this article can be found, in the online version, at doi:10.1016/j.actbio.2020.01.010.

### References

- [1] A.H. Knoll, Biomineralization and evolutionary history, Rev. Mineral. and Geochem. 54 (1) (2003) 329–356.
- [2] H.A. Lowenstam, S. Weiner, On Biomineralization, Oxford Univ. Press, Oxford, 1989
- [3] G. Falini, S. Albeck, S. Weiner, L. Addadi, Control of aragonite or calcite polymorphism by mollusk shell macromolecules, Science 271 (5245) (1996) 67–69.
- [4] L. Addadi, S. Weiner, Biomineralization: mineral formation by organisms, Physica Scripta 89 (9) (2014) 098003.
- [5] G. Falini, S. Fermani, S. Goffredo, Coral biomineralization: a focus on intra-skeletal organic matrix and calcification, Semin. Cell Dev. Biol. 46 (2015) 17–26.
- [6] J.-P. Cuif, A. Bendounan, Y. Dauphin, J. Nouet, F. Sirotti, Synchrotron-based photoelectron spectroscopy provides evidence for a molecular bond between calcium and mineralizing organic phases in invertebrate calcareous skeletons, Anal. Bioanal. Chem. 405 (27) (2013) 8739–8748.
- [7] J.E.N. Veron, Corals of the World, Australian Institute of Marine Sciences, Townsville, 2000.
- [8] T.J. Dewitt, S.M. Scheiner, Phenotypic Plasticity: Functional and Conceptual Approaches, Oxford University Press, New York, 2004.
- [9] A.R.A. Mateus, M. Marques-Pita, V. Oostra, E. Lafuente, P.M. Brakefield, B.J. Zwaan, P. Beldade, Adaptive developmental plasticity: compartmentalized responses to environmental cues and to corresponding internal signals provide phenotypic flexibility, BMC Biol. 12 (2014) 97-97.
- [10] S.F. Gilbert, Ecological developmental biology: environmental signals for normal animal development, Evol. Dev. 14 (1) (2012) 20–28.
- [11] M.P. Lesser, V.M. Weis, M.R. Patterson, P.L. Jokiel, Effects of morphology and water motion on carbon delivery and productivity in the reef coral, pocillopora damicornis (Linnaeus): diffusion barriers, inorganic carbon limitation, and biochemical plasticity, I. Exp. Mar. Biol. Ecol. 178 (2) (1994) 153–179.
- [12] T. Mass, A. Genin, Environmental versus intrinsic determination of colony symmetry in the coral pocillopora verrucosa, Mar. Ecol. Prog. Ser. 369 (2008) 131–137.
- [13] K.P. Sebens, J. Witting, B. Helmuth, Effects of water flow and branch spacing on particle capture by the reef coral *madracis mirabilis* (Duchassaing and michelotti), J. Exp. Mar. Biol. Ecol. 211 (1) (1997) 1–28.

- [14] S. Einbinder, T. Mass, E. Brokovich, Z. Dubinsky, J. Erez, D. Tchernov, Changes in morphology and diet of the coral *Stylophora pistillata* along a depth gradient, Mar. Ecol. Prog. Ser. 381 (2009) 167-174.
- [15] G. Goodbody-Gringley, J. Waletich, Morphological plasticity of the depth generalist coral, montastraea cavernosa, on mesophotic reefs in bermuda, Ecology 99 (7) (2018) 1688–1690.
- [16] B.S.T. Helmuth, K.P. Sebens, T.L. Daniel, Morphological variation in coral aggregations: branch spacing and mass flux to coral tissues, J. Exp. Mar. Biol. Ecol. 209 (1–2) (1997) 233–259.
- [17] P. Marti-Puig, Z.H. Forsman, R.D. Haverkort-Yeh, I.S.S. Knapp, J.E. Maragos, R.J. Toonen, Extreme phenotypic polymorphism in the coral genus pocillopora; micro-morphology corresponds to mitochondrial groups, while colony morphology does not, Bull. Mar. Sci. 90 (1) (2014) 211–231.
- [18] T. Mass, S. Einbinder, E. Brokovich, N. Shashar, R. Vago, J. Erez, Z. Dubinsky, Photoacclimation of *Stylophora pistillata* to light extremes: metabolism and calcification, Mar. Ecol. Prog. Ser. 334 (2007) 93–102.
- [19] G. Eyal, J. Wiedenmann, M. Grinblat, C. D'Angelo, E. Kramarsky-Winter, T. Treibitz, O. Ben-Zvi, Y. Shaked, T.B. Smith, S. Harii, V. Denis, T. Noyes, R. Tamir, Y. Loya, Spectral diversity and regulation of coral fluorescence in a mesophotic reef habitat in the red sea, PLoS One 10 (6) (2015) e0128697.
- [20] M.P. Lesser, M. Slattery, J.J. Leichter, Ecology of mesophotic coral reefs, J. Exp. Mar. Biol. Ecol. 375 (1–2) (2009) 1–8.
- [21] T. Goreau, N. Goreau, The physiology of skeleton formation in corals. II. Calcium deposition by hermatypic corals under various conditions in the reef, Biol. Bull. 117 (1959) 239–250.
- [22] S. Keshavmurthy, S.-Y. Yang, A. Alamaru, Y.-Y. Chuang, M. Pichon, D. Obura, S. Fontana, S. De Palmas, F. Stefani, F. Benzoni, A. MacDonald, A.M.E. Noreen, C. Chen, C.C. Wallace, R.M. Pillay, V. Denis, A.Y. Amri, J.D. Reimer, T. Mezaki, C. Sheppard, Y. Loya, A. Abelson, M.S. Mohammed, A.C. Baker, P.G. Mostafavi, B.A. Suharsono, C.A. Chen, DNA barcoding reveals the coral "laboratory-rat", Stylophora pistillata encompasses multiple identities, Sci. Rep. 3 (2013) 1520, doi:10.1038/srep01520.
- [23] J. Stolarski, Three-dimensional micro- and nanostructural characteristics of the scleractinian coral skeleton: a biocalcification proxy, Acta Palaeontol. Pol. 48 (3) (2003) 497–530.
- [24] B. Pokroy, A. Fitch, E. Zolotoyabko, The microstructure of biogenic calcite: a view by high-resolution synchrotron powder diffraction, Adv. Mater. 18 (18) (2006) 2363–2368.
- [25] I. Polishchuk, A.A. Bracha, L. Bloch, D. Levy, S. Kozachkevich, Y. Etinger-Geller, Y. Kauffmann, M. Burghammer, C. Giacobbe, J. Villanova, G. Hendler, C.-Y. Sun, A.J. Giuffre, M.A. Marcus, L. Kundanati, P. Zaslansky, N.M. Pugno, P.U.P.A. Gilbert, A. Katsman, B. Pokroy, Coherently aligned nanoparticles within a biogenic single crystal: a biological prestressing strategy, Science 358 (6368) (2017) 1294–1298.
- [26] J.L. Drake, T. Mass, L. Haramaty, E. Zelzion, D. Bhattacharya, P.G. Falkowski, Proteomic analysis of skeletal organic matrix from the stony coral *Stylophora pistillata*, Proc. Natl. Acad. Sci. USA 110 (10) (2013) 3788–3793.
- [27] T. Takeuchi, L. Yamada, C. Shinzato, H. Sawada, N. Satoh, Stepwise evolution of coral biomineralization revealed with genome-wide proteomics and transcriptomics, PLoS One 11 (6) (2016) e0156424.
- [28] D. Zoccola, P. Ganot, A. Bertucci, N. Caminiti-Segonds, N. Techer, C.R. Voolstra, M. Aranda, E. Tambutté, D. Allemand, J.R. Casey, S. Tambutté, b in corals point towards a key step in the evolution of cnidarian calcification, Sci. Rep. 5 (2015) 9983, doi:10.1038/srep09983.
- [29] T. Mass, J.L. Drake, L. Haramaty, J.D. Kim, E. Zelzion, D. Bhattacharya, P.G. Falkowski, Cloning and characterization of four novel coral acid-rich proteins that precipitate carbonates in vitro, Curr. Biol. 23 (12) (2013) 1126–1131.
- [30] D.W. Pfennig, M.A. Wund, E.C. Snell-Rood, T. Cruickshank, C.D. Schlichting, A.P. Moczek, Phenotypic plasticity's impacts on diversification and speciation, Trends Ecol. Evol. (Amst.) 25 (8) (2010) 459–467.
- [31] G.J. Narlikar, R. Sundaramoorthy, T. Owen-Hughes, Mechanisms and functions of ATP-dependent chromatin-remodeling enzymes, Cell 154 (3) (2013)
- [32] I. Cohen, Z. Dubinsky, Long term photoacclimation responses of the coral *Stylophora pistillata* to reciprocal deep to shallow transportation: photosynthesis and calcification. Front. Mar Sci. 2 (2015) 45.
- [33] M.P. Lesser, Coral bleaching: causes and mechanisms, in: Z. Dubinsky, N. Stambler (Eds.), Coral Reefs: An Ecosystem in Transition, Springer, Netherlands, Dordrecht, 2011, pp. 405–419.
- [34] E. Tambutte, A.A. Venn, M. Holcomb, N. Segonds, N. Techer, D. Zoccola, D. Allemand, S. Tambutte, Morphological plasticity of the coral skeleton under CO2-driven seawater acidification, Nat. Commun. 6 (2015) 7368, doi:10.1038/ ncomms8368.
- [35] S. Enríquez, E.R. Méndez, R.I. -Prieto, Multiple scattering on coral skeletons enhances light absorption by symbiotic algae, Limnol. Oceanogr. 50 (4) (2005) 1025–1032.
- [36] L.A. Marcelino, M.W. Westneat, V. Stoyneva, J. Henss, J.D. Rogers, A. Radosevich, V. Turzhitsky, M. Siple, A. Fang, T.D. Swain, J. Fung, V. Backman, Modulation of light-enhancement to symbiotic algae by light-scattering in corals and evolutionary trends in bleaching, PLoS One 8 (4) (2013) e61492.
- [37] A. Moya, S. Tambutte, A. Bertucci, E. Tambutte, S. Lotto, D. Vullo, C.T. Supuran, D. Allemand, D. Zoccola, Carbonic anhydrase in the scleractinian coral Stylophora pistillata Characterization, localization, and role in biomineralization, J. Biol. Chem. 283 (37) (2008) 25475–25484.

- [38] T. Mass, H.M. Putnam, J.L. Drake, E. Zelzion, R.D. Gates, D. Bhattacharya, P.G. Falkowski, Temporal and spatial expression patterns of biomineralization proteins during early development in the stony coral pocillopora damicornis, Proc. R. Soc. Lond. B: Biol. Sci. 283 (1829) (2016).
- [39] T. Mass, J.L. Drake, E.C. Peters, W. Jiang, P.G. Falkowski, Immunolocalization of skeletal matrix proteins in tissue and mineral of the coral *Stylophora pistillata*, Proc. Natl. Acad. Sci. 111 (35) (2014) 12728–12733.
- [40] E. Tambutte, D. Allemand, E. Mueller, J. Jaubert, A compartmental approach to the mechanism of calcification in hermatypic corals, J. Exp. Biol. 199 (5) (1996) 1029–1041.
- [41] D. Bhattacharya, S. Agrawal, M. Aranda, S. Baumgarten, M. Belcaid, J.L. Drake, D. Erwin, S. Foret, R.D. Gates, D.F. Gruber, B. Kamel, M.P. Lesser, O. Levy, Y.J. Liew, M. MacManes, T. Mass, M. Medina, S. Mehr, E. Meyer, D.C. Price, H.M. Putnam, H. Qiu, C. Shinzato, E. Shoguchi, A.J. Stokes, S. Tambutté, D. Tchernov, C.R. Voolstra, N. Wagner, C.W. Walker, A.P.M. Weber, V. Weis, E. Zelzion, D. Zoccola, P.G. Falkowski, Comparative genomics explains the evolutionary success of reef-forming corals, Elife 5 (2016) e13288.
- [42] P.W. Glynn, L. D'Croz, Experimental evidence for high temperature stress as the cause of el niño-coincident coral mortality, Coral Reefs 8 (4) (1990) 181–191.
- [43] A.H. Knoll, R.K. Bambach, J.L. Payne, S. Pruss, W.W. Fischer, Paleophysiology and end-Permian mass extinction, Earth Planet. Sci. Lett. 256 (3) (2007) 295–313.
- [44] T.P. Hughes, A.H. Baird, D.R. Bellwood, M. Card, S.R. Connolly, C. Folke, R. Grosberg, O. Hoegh-Guldberg, J.B.C. Jackson, J. Kleypas, J.M. Lough, P. Marshall, M. Nystrom, S.R. Palumbi, J.M. Pandolfi, B. Rosen, J. Roughgarden, Climate change, human impacts, and the resilience of coral reefs, Science 301 (5635) (2003) 929–933
- [45] D.P. Tittensor, C. Mora, W. Jetz, H.K. Lotze, D. Ricard, E.V. Berghe, B. Worm, Global patterns and predictors of marine biodiversity across taxa, Nature 466 (2010) 1098.
- [46] J. Stolarski, M.V. Kitahara, D.J. Miller, S.D. Cairns, M. Mazur, A. Meibom, The ancient evolutionary origins of scleractinia revealed by azooxanthellate corals, BMC Evol. Biol. 11 (1) (2011) 316.
- [47] M.V. Kitahara, S.D. Cairns, J. Stolarski, D. Blair, D.J. Miller, A comprehensive phylogenetic analysis of the scleractinia (Cnidaria, anthozoa) based on mitochondrial CO1 sequence data, PLoS One 5 (7) (2010) e11490.
- [48] M. Hasegawa, H. Kishino, T. Yano, Dating of the human-ape splitting by a molecular clock of mitochondrial DNA, J. Mol. Evol. 22 (2) (1985) 160–174.
- [49] S. Kumar, G. Stecher, K. Tamura, MEGA7: molecular evolutionary genetics analysis version 7.0 for bigger datasets, Mol. Biol. Evol. 33 (7) (2016) 1870–1874.
- [50] J. Schindelin, I. Arganda-Carreras, E. Frise, V. Kaynig, M. Longair, T. Pietzsch, S. Preibisch, C. Rueden, S. Saalfeld, B. Schmid, J.-Y. Tinevez, D.J. White, V. Hartenstein, K. Eliceiri, P. Tomancak, A. Cardona, Fiji: an open-source platform for biological-image analysis, Nat. Methods 9 (7) (2012) 676–682.
- [51] G.L. Cowie, J.I. Hedges, Sources and reactivities of amino acids in a coastal marine environment, Limnol. Oceanogr. 37 (4) (1992) 703–724.
- [52] A.M. Bolger, M. Lohse, B. Usadel, Trimmomatic: a flexible trimmer for illumina sequence data, Bioinformatics 30 (15) (2014) 2114–2120.
- [53] J. Bengtsson-Palme, M. Hartmann, K.M. Eriksson, C. Pal, K. Thorell, D.G. Larsson, R.H. Nilsson, METAXA2: improved identification and taxonomic classification of small and large subunit rRNA in metagenomic data, Mol. Ecol. Resour. 15 (6) (2015) 1403–1414.
- [54] A. Dobin, C.A. Davis, F. Schlesinger, J. Drenkow, C. Zaleski, S. Jha, P. Batut, M. Chaisson, T.R. Gingeras, STAR: ultrafast universal RNA-seq aligner, Bioinformatics 29 (1) (2013) 15–21.
- [55] M.I. Love, W. Huber, S. Anders, Moderated estimation of fold change and dispersion for RNA-Seq data with DESeq2, Genome Biol. 15 (12) (2014) 550.
- [56] M.D. Young, M.J. Wakefield, G.K. Smyth, A. Oshlack, Gene ontology analysis for RNA-seq: accounting for selection bias, Genome Biol 11 (2) (2010) R14.
- [57] A.A. Sergushichev, An algorithm for fast preranked gene set enrichment analysis using cumulative statistic calculation, bioRxiv (2016) 060012.
- [58] A. Subramanian, P. Tamayo, V.K. Mootha, S. Mukherjee, B.L. Ebert, M.A. Gillette, A. Paulovich, S.L. Pomeroy, T.R. Golub, E.S. Lander, J.P. Mesirov, Gene set enrichment analysis: a knowledge-based approach for interpreting genome-wide expression profiles, Proc. Natl. Acad. Sci. USA 102 (43) (2005) 15545– 15550.
- [59] C.R. Voolstra, Y. Li, Y.J. Liew, S. Baumgarten, D. Zoccola, J.-F. Flot, S. Tambutté, D. Allemand, M. Aranda, Comparative analysis of the genomes of *Stylophora* pistillata and Acropora digitifera provides evidence for extensive differences between species of corals, Sci. Rep. 7 (1) (2017) 17583.
- [60] C. Shinzato, E. Shoguchi, T. Kawashima, M. Hamada, K. Hisata, M. Tanaka, M. Fujie, M. Fujiwara, R. Koyanagi, T. Ikuta, A. Fujiyama, D.J. Miller, N. Satoh, Using the acropora digitifera genome to understand coral responses to environmental change, Nature 476 (2011) 320–323.
- [61] D. Bhattacharya, S. Agrawal, M. Aranda, S. Baumgarten, J.L.D. Mahdi Belcaid, D. Erwin, S. Foret, R.D. Gates, D.F. Gruber, B. Hanna, M.P. Lesser, O. Levy, Yi Jin Liew, M. MacManes, T. Mass, M. Medina, S. Mehr, E. Meyer, D.C. Price, H.M. Putnam, H. Qiu, C. Shinzato, E. Shoguchi, A.J. Stokes, S. Tambutté, D. Tchernov, C.R. Voolstra, N. Wagner, C.W. Walker, A.P.M. Weber, V. Weiss, E. Zelzion, D. Zoccola, P.G. Falkowski, Basis for ecological success of reef-forming corals elucidated using comparative genomics, eLife 5 (2016) e13288, doi:10.7554/eLife.13288.

- [62] D.M. Emms, S. Kelly, OrthoFinder: solving fundamental biases in whole genome comparisons dramatically improves orthogroup inference accuracy, Genome Biol. 16 (2015) 157.
- Genome Biol. 16 (2015) 157.
  [63] D.M. Emms, S. Kelly, OrthoFinder: phylogenetic orthology inference for comparative genomics, Genome Biol. 20 (1) (2019) 238.
  [64] J. Zhang, K. Kobert, T. Flouri, A. Stamatakis, PEAR: a fast and accurate illumina paired-end reAd mergeR, Bioinformatics 30 (5) (2014) 614–620.
- [65] K. Katoh, D.M. Standley, MAFFT multiple sequence alignment software version 7: improvements in performance and usability, Mol. Biol. Evol. 30 (4) (2013) 772–780.
- [66] A. Criscuolo, S. Gribaldo, BMGE (Block mapping and gathering with entropy): a new software for selection of phylogenetic informative regions from multiple sequence alignments, BMC Evol. Biol. 10 (2010) 210.
- [67] L.T. Nguyen, H.A. Schmidt, A. von Haeseler, B.Q. Minh, IQ-TREE: a fast and effective stochastic algorithm for estimating maximum-likelihood phylogenies, Mol. Biol. Evol. 32 (1) (2015) 268–274.
  [68] M. Hasegawa, H. Kishino, T. Yano, Dating of the human-ape splitting by a molecular clock of mitochondrial dna, J. Mol. Evol. 22 (2) (1985) 160–174.